Observing the Coulomb shifts of ionization times in high-order harmonic generation

Shengjun Yue,[1,2,3] Jin Liu,[1,2] Shan Xue,[1,2] Hongchuan Du,[1,2,*] and Manfred Lein[3,†]

[1] *Frontiers Science Center for Rare Isotopes, Lanzhou University, Lanzhou 730000, China*
[2] *School of Nuclear Science and Technology, Lanzhou University, Lanzhou 730000, China*
[3] *Leibniz University Hannover, Institute of Theoretical Physics, Appelstraße 2, 30167 Hannover, Germany*

(Dated: May 20, 2023)

The Coulomb interaction between the active electron and the parent ion is inherent in high-order harmonic generation from laser-driven atoms, but it is often neglected in modeling the electron dynamics. For this reason, the pioneering measurement scheme based on orthogonally polarized two-color fields reported in [Nature (London) 485, 343 (2012)], which is able to measure ionization and return times for the electron trajectories, does not reflect the time shifts caused by the Coulomb interaction. We introduce a simple Coulomb correction to the electron motion in the two-color scheme, leading to modified retrieval equations for the extraction of time information from the observables. We apply the modified equations to data calculated from simulations of the time-dependent Schrödinger equation and we show that the scheme effectively reveals the Coulomb shift of the ionization time.

I. INTRODUCTION

Resolving ultrafast dynamics of the microworld on their natural time scale is the aim of ultrafast detection. Thanks to the development of strong-field physics over the past decades, ultrafast detection has broken through the femtosecond limit, thus opening the door of attosecond science [1]. High-order harmonic generation (HHG), which stands for the nonlinear and nonperturbative response to strong fields, causes emission of radiation that carries information on ultrafast dynamics and hence it has numerous applications for probing the dynamics in atoms, molecules, and solids [2–8]. The classical physical picture of the HHG process is described by the three-step model [9, 10] consisting of ionization, followed by acceleration and return of the electron, which then recombines with the parent ion. The quantum-mechanical version of the three-step model is known as the strong-field approximation (SFA) or Lewenstein model [11]. Its formulation in terms of complex-valued electron trajectories is known as the quantum-orbit (QO) model [12].

The measurement of the times of ionization and return (recombination) is an important topic in HHG. It deepens our understanding of the mechanism of HHG in terms of trajectories, but it also has practical implications. For example, the understanding of spectral caustics requires the accurate knowledge of electron trajectories [13–15]. More generally, the time structure of the trajectories is needed for the application of high-harmonic spectroscopy (HHS) to dynamical problems. HHS refers to the extraction of static and dynamical properties of atoms, molecules, and condensed phases from the HHG signal. For example, trajectory-resolved HHS can be used to investigate the motion of nuclei in molecules [4, 16, 17], dynamical symmetries [6, 18], and the evolution of electronic wavepackets under the tunneling barrier [19, 20]. The accuracy of these measurements depends on well-defined ionization and return times.

Orthogonally polarized two-color (OTC) fields are frequently applied for manipulating electron trajectories or wavepackets [21–25]. They provide a method to retrieve both ionization and return times in HHG [26]: A weak second-harmonic streaking field, polarized perpendicular to the driving field, is used to disturb the electron trajectory after ionization. In this scheme, there are two key observables: the harmonic intensity and the ratio of the components of the harmonics polarized in the two orthogonal directions. By measuring these observables as a function of the relative phase between the two fields and invoking a classical-trajectory analysis ("displacement gate" and "velocity gate"), the ionization and return times can be determined for each harmonic order. The OTC scheme has been extended to complex-time trajectories in Ref. [27]. The ionization and return times extracted from the ω–2ω OTC scheme using the original (Coulomb-free) displacement gate and velocity gate agree very well with the QO model. Considering that the QO model neglects the Coulomb interaction between the electron and the parent ion, this finding implies that the original trajectory analysis of the ω–2ω data does not give access to Coulomb effects on the ionization and return times.

The Coulomb potential is known to significantly influence strong-field ionization and HHG [28–36]. It has been shown that the Coulomb potential can lead to an ionization-time shift of about 35 attoseconds in HHG [33], which is not observed when using the above-described ω–2ω OTC scheme. Recently, we have analyzed this issue and found that streaking with higher frequencies such as 4ω rather than 2ω remedies the problem and provides the correct Coulomb-shifted times [35]. The advantage of the high-frequency method is that no knowledge about the Coulomb interaction is needed in the formulation of the retrieval equations that are used to extract the times from the observables. The drawback, however, is that the experimental implementation

* duhch@lzu.edu.cn
† lein@itp.uni-hannover.de

of a higher streaking frequency is substantially more challenging than the ω–2ω scheme.

In this work, we refine the theoretical model underlying the OTC probe method by incorporating the Coulomb interaction into the dynamics in the direction of the probe polarization. We then apply the method to data obtained by solving the time-dependent Schrödinger equation (TDSE). With the modified retrieval equations, we find that the resulting ionization time includes the Coulomb-induced shift. This means that effectively, the scheme has improved temporal measurement accuracy and thus extends the universality of the original OTC scheme. In other words, while the information about Coulomb shifts is present in the ω–2ω two-color data, a careful analysis is required to extract it.

In Section II we present the details of the TDSE and Gabor transform, which is applied to isolate the short HHG trajectory. In Section III, we introduce the Coulomb corrections to the OTC method. We then apply the modified retrieval equations to reconstruct the time information in Section IV. Section V concludes our work.

II. NUMERICAL MODEL

The model system for the TDSE simulations is the same as in the previous work [35] and the simulation parameters are similar. For completeness, we briefly repeat the main points. The dynamics of the helium model atom interacting with two-color fields is described by solving the TDSE in the single-active-electron approximation for a two-dimensional (2D) potential $V(\mathbf{r}) = -1/\sqrt{\mathbf{r}^2 + a}$, where $\mathbf{r} = [x\ y]^{\mathrm{T}}$ is the electron position and the softcore parameter $a = 0.0684$ a.u. is chosen to reproduce the ionization potential of helium, i.e., $I_p = 24.6$ eV. In the length gauge, the TDSE reads (Hartree atomic units are used unless otherwise stated)

$$i\frac{\partial}{\partial t}\psi = \left[-\frac{1}{2}\left(\frac{\partial^2}{\partial x^2} + \frac{\partial^2}{\partial y^2}\right) + V(\mathbf{r}) + \mathbf{r}\cdot\mathbf{E}(t)\right]\psi. \quad (1)$$

The OTC field $\mathbf{E}(t) = -\dot{\mathbf{A}}(t)$ follows from the vector potential

$$\mathbf{A}(t) = -\frac{E_0}{\omega} f(t) \begin{bmatrix} \sin(\omega t) \\ \frac{\epsilon}{n}\sin(n\omega t + \phi) \end{bmatrix}. \quad (2)$$

Throughout the paper, we use indices x and y to denote the two components of a vector. E_0 and ω are the field amplitude and the frequency of the fundamental laser pulse. The relative amplitude ϵ is set to 0.02. The two-color delay ϕ is the relative phase between the main driving field polarized along the x-axis and the perturbing probe field (streaking field) polarized along the y-axis. The factor n ($n \in \mathbb{R}$, $n > 0$) determines the streaking frequency $n\omega$. The envelope $f(t)$ consists of a one-cycle rising edge, one-cycle flattop, and one-cycle falling edge. The range of the laser pulse is from $-T$ to $2T$ with the optical period $T = 2\pi/\omega$ so that $t = 0$ is the beginning of the flattop region. We use a ramp of the form $\cos^6(\omega t/4)$ for the leading edge ($-T \le t \le 0$) and $\sin^6(\omega t/4)$ for the trailing edge ($T \le t \le 2T$).

We solve the 2D TDSE using the Crank-Nicolson method [37, 38] with a time step of 0.02 a.u. The Cartesian grid has the size $L_x \times L_y = 300 \times 160$ a.u. with 3000×1600 grid points. A mask function $M(x)$ along the x-axis with $M(x) = \cos^{1/8}\left(\pi\left(|x| - x_0\right)/\left(L_x - 2x_0\right)\right)$ for $|x| \ge x_0$ and $M(x) = 1$ for $|x| \le x_0$ is applied to absorb the wavefunction at the boundary, where we set $x_0 = 1.1E_0/\omega^2$. For the y-direction, we apply a similar treatment with $y_0 = (7/18)L_y$. From the time-dependent wavefunction, the dipole acceleration is calculated via the Ehrenfest theorem [39],

$$\mathbf{a}(t) = \langle\psi|\,\partial_{\mathbf{r}} V(\mathbf{r}) + \mathbf{E}(t)\,|\psi\rangle\,. \quad (3)$$

The high-harmonic spectrum cannot be directly used as an observable for the time retrieval because there are two types of electron trajectories contributing to the same harmonic order, known as the "short" and "long" trajectories, and their interference significantly affects the harmonic radiation [12]. In experiments, the short trajectory can be selected by setting appropriate macroscopic conditions [4, 40, 41]. On the theory side, we use the Gabor transform to isolate the short trajectory [6, 42, 43]. The total Gabor intensity $I_G(\Omega, t) = I_{G_x}(\Omega, t) + I_{G_y}(\Omega, t)$ reads

$$I_G(\Omega, t) = \sum_{j=x,y}\left|\int dt' a_j(t')\, e^{-\left(t'-t\right)^2/\left(2\sigma^2\right)+i\Omega t'}\right|^2, \quad (4)$$

with the harmonic frequency Ω and $\sigma = 1/(3\omega)$. To ensure the distinguishability of electron trajectories, we limit the analysis to the plateau region with harmonic orders between the 20th and 60th for the short trajectory. For any given harmonic frequency Ω, we find the time t_e that corresponds to the maximum of the time-dependent function $I_G(\Omega, t)$. We interpret t_e as the emission time for the given value of Ω. The time t_e is within the range of $[0.3T, 0.7T]$ for the short trajectory. It serves only to obtain the harmonic intensity $I_G(\Omega, t_e)$ and the amplitude ratio $R(\Omega) = \sqrt{I_{G_y}(\Omega, t_e)/I_{G_x}(\Omega, t_e)}$ of the components polarized along y and x. These are two measurable observables that depend on the two-color delay and on the streaking frequency.

III. COULOMB CORRECTIONS FOR THE TIME-RETRIEVAL EQUATIONS

After obtaining the measurable quantities, it is necessary to relate these observables to the ionization and return times via a theoretical model. The original analysis in Refs. [26, 27] is based on the assumption that the electron follows a Newtonian trajectory such that the force along the probe field direction (orthogonal to the main driving field) arises from the probe field alone and does

not include the Coulomb interaction. Furthermore, the probe field is chosen weak enough to ensure that the ionization and return times are determined purely by the longitudinal dynamics along the fundamental field and they are not altered by the probe field. However, the effect of the Coulomb interaction on the electron motion in the probe-field direction cannot necessarily be ignored. In the present work, we use a Coulomb-corrected Newtonian trajectory to deduce the retrieval equations for obtaining the ionization and return times. In principle, when assuming a monochromatic field, i.e., $f(t) \equiv 1$, the lateral electron trajectory $y(t)$ obeys Newton's second law in the form

$$\ddot{y}(t) = -\epsilon\, E_0 \cos(n\omega t + \phi) - \frac{\partial V_c}{\partial y}, \tag{5}$$

where the Coulomb force $-\partial V_c/\partial y$ follows from the Coulomb potential V_c. We assume that the ionization time t_i may be complex. In this case, we follow the usual interpretation that the time path from t_i to $\mathrm{Re}\, t_i$ corresponds to tunneling of the electron through the laser-induced potential barrier until it reaches the tunnel exit at $t = \mathrm{Re}\, t_i$. For the tunneling path between t_i and $\mathrm{Re}\, t_i$, we neglect the Coulomb interaction (this is justified by the good agreement between the classical models and the analytical R-matrix theory, ARM, see Section IV) so that the velocity is

$$\dot{y}\,(t) = v_{y0} - \frac{\epsilon E_0}{n\omega}\left[\sin(n\omega t + \phi) - \sin(n\omega t_i + \phi)\right] \tag{6}$$

with the initial lateral velocity v_{y0} at the ionization time. For real times $t > \mathrm{Re}\, t_i$, we assume that the Coulomb term in Eq. (5) is relevant only for a short time compared to the laser period so that the Coulomb-induced momentum change of the electron can be approximated as a short kick. The magnitude of the Coulomb kick Δv_y can be calculated by treating the electric field as constant, which leads to [44]

$$\Delta v_y = \frac{\epsilon\, \pi E_0 \cos\left(n\omega\, \mathrm{Re}\, t_i + \phi\right)}{\left(2I_p\right)^{3/2}}. \tag{7}$$

Hence, for times $t > \mathrm{Re}\, t_i$, we have the lateral velocity

$$\begin{aligned}\dot{y}\,(t) = v_{y0} - \frac{\epsilon E_0}{n\omega}\left[\sin(n\omega t + \phi) - \sin\,(n\omega t_i + \phi)\right] \\ + \Delta v_y\end{aligned} \tag{8}$$

Integrating Eqs. (6),(8) from t_i to t and applying the initial condition $y(t_i) = 0$, the lateral electron trajectory for $t > \mathrm{Re}\, t_i$ is

$$\begin{aligned} y\,(t) &= v_{y0}\,(t - t_i) + \Delta v_y\,(t - \mathrm{Re}\, t_i) \\ &+ \frac{\epsilon E_0}{(n\omega)^2}\left[\cos(n\omega t + \phi) - \cos(n\omega t_i + \phi)\right] \\ &+ \frac{\epsilon E_0}{n\omega}\sin(n\omega t_i + \phi)\,(t - t_i)\,. \end{aligned} \tag{9}$$

The return time t_r of the electron may be complex so that the final part of the electron trajectory lasts from $\mathrm{Re}\, t_r$ to t_r [33] and the expressions above need to be extended to complex arguments t. However, we will neglect the (usually small) imaginary part of t_r in the retrieval equations below.

The use of complex times is motivated by the QO model [12]. In the QO model, complex times t_i, t_r are obtained as solutions of the saddle-point equations

$$\mathbf{v}^2(t_i)/2 = -I_p, \quad \mathbf{v}^2(t_r)/2 = \Omega - I_p, \tag{10}$$

where the electron velocity is $\mathbf{v}(t) = \mathbf{p} + \mathbf{A}(t)$ with the saddle-point momentum $\mathbf{p} = -1/(t_r - t_i)\int_{t_i}^{t_r}\mathbf{A}(t)dt$. As a consequence of the weak amplitude of the probe field, the lateral components (v_y, p_y, and $A_y(t)$) are negligible in Eq. (10) as far as the calculation of the times t_i, t_r is concerned. These saddle-point equations result from finding the stationary points of the action $S = \int_{t_i}^{t_r} dt\left[\mathbf{v}^2(t)/2 + I_p\right]$. The QO model is a Coulomb-free theory; in the results below it will be used only as a reference theory, while our actual aim is the retrieval of ionization and return times in the presence of the Coulomb interaction. When the ionization potential I_p is set to zero in the first equation of the QO model, i.e., when setting $\mathbf{v}^2(t_i)/2 = 0$, we arrive at the so-called simple man's model, in which all times are real and the trajectories are classical [9].

To generate high harmonics by recombination, the recollision condition $y(t_r) - y(t_i) = 0$ has to be met. Therefore, from Eq. (9), the required initial lateral velocity is

$$\begin{aligned} v_{y0} = &-\frac{\epsilon E_0}{n\omega}\left[\sin(\varphi_i) + \frac{\cos(\varphi_r) - \cos(\varphi_i)}{n\omega\,(t_r - t_i)}\right] \\ &- \frac{\Delta v_y\,(t_r - \mathrm{Re}\, t_i)}{t_r - t_i}, \end{aligned} \tag{11}$$

with $\varphi_i = n\omega t_i + \phi$ and $\varphi_r = n\omega t_r + \phi$. The strongest HHG signal is obtained for vanishing real part of the initial lateral velocity, $\mathrm{Re}\, v_{y0} = 0$ [27, 45, 46].

In the trajectory picture, the amplitude ratio R defined in Section II is determined by the ratio of the return velocity components in y- and x-directions [27], $R = |\dot{y}(t_r)/\dot{x}(t_r)|$. Here $\dot{x}(t_r) = \sqrt{2\,(\Omega - I_p)}$ is the x-component of the return velocity, where we neglect the small effect of the probe field. Inserting Eq. (11) into Eq. (8), we have

$$\begin{aligned} \dot{y}\,(t) &= \mathcal{M}\left[\sin(\varphi_i) + \frac{\cos(\varphi_r) - \cos(\varphi_i)}{n\omega\,(t_r - t_i)}\right] - \frac{\Delta v_y\,(t_r - \mathrm{Re}\, t_i)}{t_r - t_i} \\ &+ \mathcal{M}\left[\sin(n\omega t + \phi) - \sin\,(\varphi_i)\right] + \Delta v_y \\ &= \mathcal{M}\left[\sin(n\omega t + \phi) + \frac{\cos(\varphi_r) - \cos(\varphi_i)}{n\omega\,(t_r - t_i)}\right] \\ &- \Delta v_y \frac{i\,\mathrm{Im} t_i}{t_r - t_i}, \end{aligned} \tag{12}$$

with $\mathcal{M} = -\epsilon E_0/\,(n\omega)$, leading to the the return velocity

at t_r

$$\dot{y}(t_r) = -\frac{\epsilon E_0}{n\omega}\left[\sin(\varphi_r) + \frac{\cos(\varphi_r)-\cos(\varphi_i)}{n\omega\,(t_r-t_i)}\right] - \Delta v_y \frac{i\,\mathrm{Im}t_i}{t_r-t_i}. \quad (13)$$

Therefore R can be written as

$$R = \frac{\epsilon E_0/(n\omega)}{\sqrt{2\,(\Omega-I_p)}}\times \left|\sin(\varphi_r) + \frac{\cos(\varphi_r)-\cos(\varphi_i)}{n\omega\,(t_r-t_i)} + \frac{\Delta v_y n\omega i\,\mathrm{Im}t_i}{\epsilon E_0(t_r-t_i)}\right|. \quad (14)$$

In the ω–2ω experiments, the measured amplitude ratio R is the square root of the intensity ratio of adjacent odd and even harmonics [26, 47].

Analogous to the terminology in [26, 27], Eqs. (11) and (14) may be termed Coulomb-corrected displacement gate and velocity gate. Compared to the two gates in Refs. [26, 27], Coulomb corrections are included through the Coulomb kick Δv_y appearing in the last terms in Eqs. (11) and (14). These two gates establish a direct connection between the observables and the two times t_r, t_i. If we know (from experiment or simulation) the two-color delay that gives the strongest harmonic intensity and the two-color delay that maximizes the amplitude ratio R, both times can be retrieved. The corresponding two retrieval equations have the form

$$\mathrm{Re}\,v_{y0} = 0, \qquad \partial R/\partial\phi = 0. \quad (15)$$

In principle, Eq. (15) is a system of two equations with four unknowns: $\mathrm{Re}\,t_i$, $\mathrm{Im}\,t_i$, $\mathrm{Re}\,t_r$, and $\mathrm{Im}\,t_r$. However, in good approximation [27, 48], we can neglect the imaginary part of t_r and substitute the imaginary part of t_i with the Keldysh time [49] at the instantaneous time $\mathrm{Re}\,t_i$, i.e., $\mathrm{Im}\,t_i = \sqrt{2I_p}/\,|E_x(\mathrm{Re}\,t_i)|$. With these simplifications, there are only two unknowns in Eq. (15), namely the real parts of t_i and t_r, which are interpreted as the physical ionization and return times. These two quantities can be found by solving the system of two equations in Eq. (15).

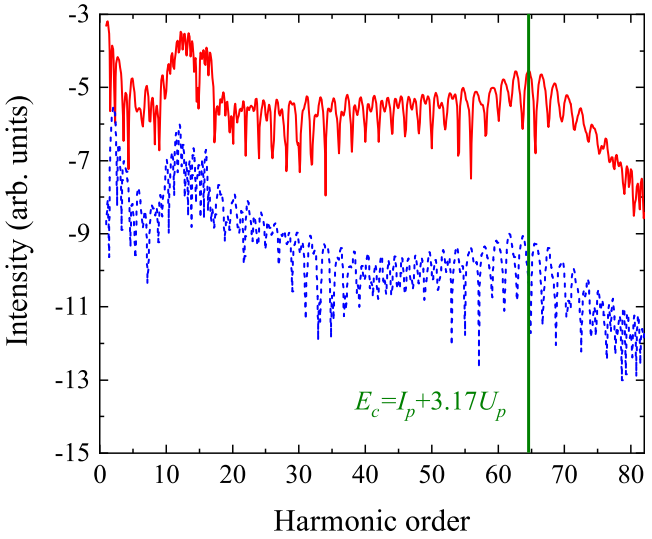

FIG. 1. The harmonic spectra polarized along the x-direction (red solid curve) and along the y-direction (blue dashed curve) calculated for the helium model atom driven by an ω–2ω field with $\omega = 0.057$ a.u., $E_0 = 0.1068$ a.u., $\phi = 0$, calculated as $P_j(\Omega) = \left|\int a_j(t)\exp(i\Omega t)\,dt\right|^2$ with $j = x, y$.

IV. RESULTS

The two-color HHG spectra are shown in Fig. 1 for an 800 nm fundamental field with intensity 4.0×10^{14} W/cm^2 and a probe field with two-color delay $\phi = 0$ and $n = 2$. The red and blue lines represent the x- and y-components, respectively. Due to the low probe-field amplitude (2% of the main field), the harmonic intensity polarized along the y-axis is much weaker. Both spectra exhibit a plateau from the 20th to the 65th harmonic order, followed by a cutoff near the expected energy value $E_c = I_p + 3.17U_p$, where $U_p = E_0^2/\left(4\omega^2\right)$ is the ponderomotive energy.

The two observables used for the further analysis are shown in Fig. 2. These data result from TDSE simulations for an ω–2ω laser field. The harmonic intensity (left panel) and the y-to-x amplitude ratio R (right panel) depend on the two-color delay. For each harmonic order, we can find the optimal phase ϕ_h maximizing the harmonic intensity [green dashed-dotted line in Fig. 2(a)] and the optimal phase ϕ_a maximizing the amplitude ratio [green dashed-dotted line in Fig. 2(b)]. The white solid lines, which are very close to the TDSE results, are the optimal phases from the Coulomb-free two-color SFA model

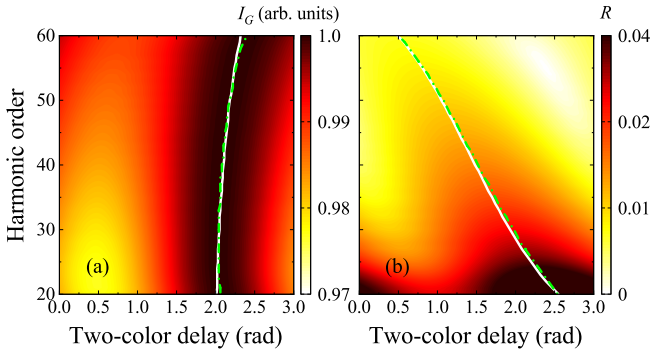

FIG. 2. TDSE results using ω–2ω fields: the normalized harmonic intensity (a) and the amplitude ratio (b) are shown in color density as functions of the harmonic order and the two-color delay. The optimal phases that maximize the observables are shown as white solid curves (SFA) and green dashed-dotted curves (TDSE). The fundamental driving field is the same as in Fig. 1.

where the harmonic intensity is calculated as

$$I_s = \left| e^{-i(S-\Omega t_r)} \right|^2 \tag{16}$$

with the action $S = \int_{t_i}^{t_r} dt \left[\mathbf{v}^2(t)/2 + I_p \right]$ evaluated at the one-color saddle-point times t_i, t_r of the QO model, but with the two-color field included in the evaluation of $\mathbf{v}$. Solving Eq. (15) with the input values ϕ_h and ϕ_a from the TDSE gives access to the real parts of ionization and return times.

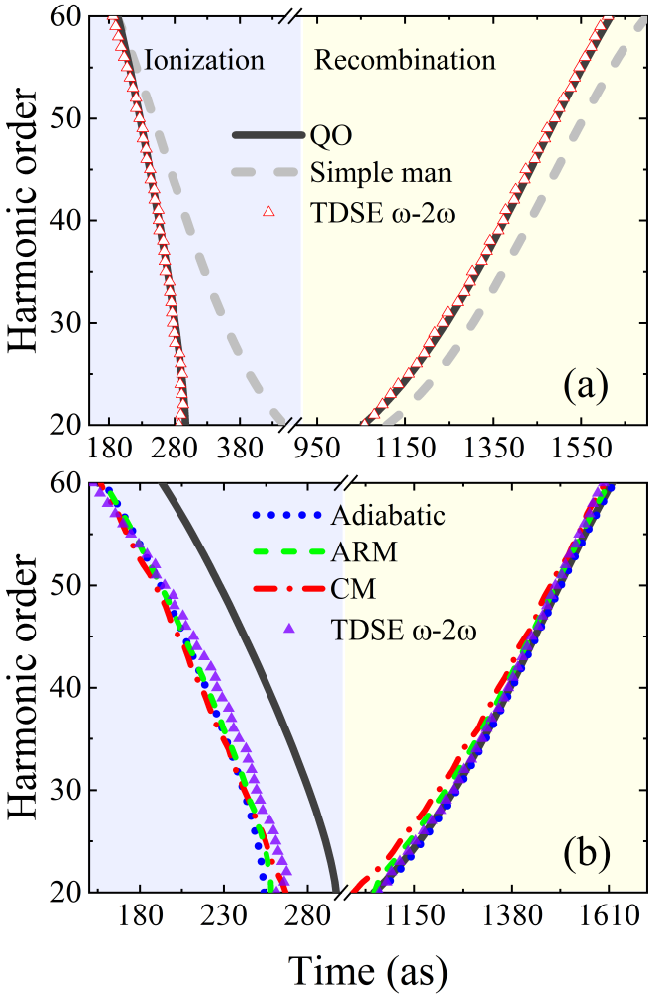

FIG. 3. Ionization and return times reconstructed from the ω–2ω TDSE results. (a) Results based on the Coulomb-free OTC scheme shown as red empty triangles; (b) results based on the Coulomb-corrected OTC scheme shown as violet triangles. The black solid lines represent the real parts of the times from the Coulomb-free QO model. The light-gray dashed line shows the times from the simple man's model. Furthermore, ionization and return times from various models with Coulomb interaction are shown: ARM (green dashed lines), CM (red dashed-dotted lines), and the adiabatic model (blue dotted lines). The laser parameters are same as in Fig. 2. Light-blue and light-yellow shaded areas show the temporal regions of ionization and recombination, respectively.

Previous studies [26, 27] show that the reconstructed ionization and return times using ω–2ω OTC fields are consistent with the QO model when the Coulomb-free retrieval equations are used. This agreement indicates that the extracted times lack Coulomb effects. This is also reflected by the fact that the optimal phases obtained from TDSE and SFA match well in Fig. 2. Figure 3(a) shows the times extracted via the Coulomb-free retrieval equations, i.e., using Eqs. (11), (14), (15) with $\Delta v_y \equiv 0$, in the case of ω–2ω fields. Indeed, the times from TDSE agree closely with the real parts of the saddle-point times from the QO model. For completeness, the figure shows also the results from the simple man's model, which are significantly different.

The retrieved ionization and return times using the Coulomb-corrected equations [Eqs. (7), (11), (14), (15)] are shown in Fig. 3(b). While the return times are almost unchanged, the ionization times are shifted by roughly 30 attoseconds to earlier times. To assess these results, we compare with three different models that quantify the influence of the Coulomb interaction on the times when only the fundamental field is considered: a full description of the classical model (CM) and the analytical R-matrix (ARM) theory is given in Refs. [33, 35, 36]; the details of the adiabatic model are given in the appendix. Besides the specific results shown below, we have checked that there is good agreement between the models in the region of Keldysh parameters $\gamma < 1$. For the ionization time (light blue shaded area in the left part of the plot), the results from CM, ARM, and the adiabatic model agree very well with each other. These models indicate that the attractive Coulomb force shifts ionization by about 35 attoseconds to earlier times. The match with

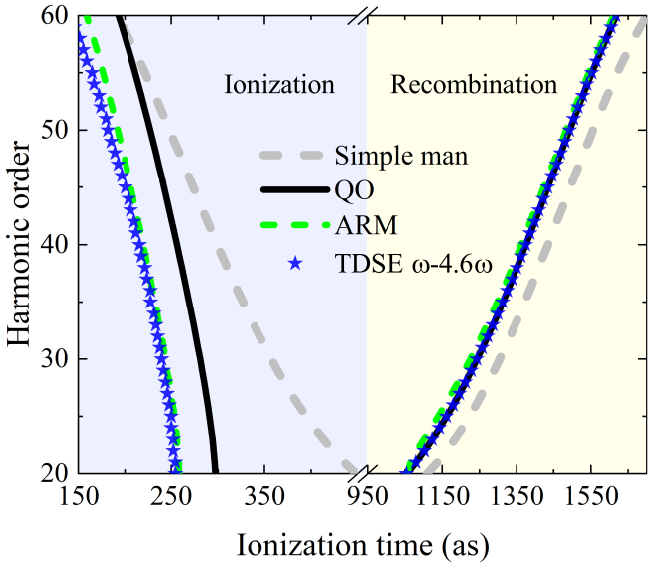

FIG. 4. Ionization and return times from TDSE with an ω–4.6ω field (blue stars) compared to ARM (greed dashed lines), QO (black lines) and the simple man's model (light-gray dashed lines).

the Coulomb-corrected ω–2ω TDSE results is particularly good at high harmonic orders. At lower harmonic orders, the match is still good with the two-color results being a few attoseconds behind the model predictions. For the return time (light yellow shaded area in the right part of the plot), we find: (i) the TDSE nearly coincides with the adiabatic model and the QO model; (ii) ARM theory shows a shift of 3-10 attoseconds when compared to the QO model, which was already reported in Ref. [33]; (iii) the time shift of the CM varies between ∼10 and ∼45 attoseconds, decreasing with increasing harmonic order. Overall, the return time is less affected by the Coulomb potential than the ionization time. In view of ARM theory being a quantum-mechanical model that includes the Coulomb interaction both in the under-barrier motion and in the subsequent unbound motion, it can be considered as the most accurate of the three models. This is consistent with the good agreement between ARM theory and the two-color TDSE for the return time. The CM and the adiabatic model, on the other hand, although being slightly less accurate, have the benefit of providing a simple interpretation of the Coulomb shift: the electron must appear earlier so that the attractive Coulomb force is compensated by additional field acceleration [35, 36]. Overall, we can conclude that the Coulomb correction for the OTC method is reasonable and that the modified equations successfully reveal the Coulomb time shift.

We also apply the modified retrieval equations to the case of high-frequency streaking. Figure 4 displays the times obtained from TDSE data via the Coulomb-corrected scheme with an ω–4.6ω field, shown as blue stars. Obviously, both ionization and return times are in line with the ARM results. In our previous work [35], we found that, even without the Coulomb correction, the high-frequency OTC method is able to measure the Coulomb time shift well, see Fig. 2 in Ref. [35]. When the Coulomb correction is included, our results show that both low and high streaking frequencies can be used to perform an accurate measurement.

V. CONCLUSIONS

In summary, we have modified the OTC scheme for probing ionization and return times in HHG by employing Coulomb-corrected Newtonian trajectories. From a measurement of the harmonic intensity and the y-to-x amplitude ratio as a function of the two-color delay, the times can be retrieved. Compared to the Coulomb-free displacement gate and velocity gate in Refs. [26, 27], the modified scheme correctly recovers the Coulomb shift of the ionization time in HHG and therefore it can be considered more reliable. The correctness of the Coulomb shift retrieved from TDSE results is shown by the comparison with three different models that all give similar results for the ionization time. One of these models is the analytical R-matrix theory, first proposed and used in [33] to evaluate the Coulomb shifts. While the required experimental observables are the same as in the OTC scheme of [26, 27], the analysis introduced in the present work differs in the equations that are used to extract the ionization time. The success of the scheme holds no matter whether a low or high streaking frequency is used. While the high-frequency streaking method (probe frequencies of about 4ω or higher) works well even without the modification of the retrieval equations, as shown in [35], the "low-frequency method" (ω–2ω) needs the Coulomb modification. We note that the ω–2ω method is easier to use in an actual experiment. It is important to note that the Coulomb correction in the time-retrieval equations refers to the component of the electron motion along the probe field, which is orthogonal to the strong fundamental driving field, whereas the Coulomb shift of the ionization time is due to the Coulomb effect on the motion along the fundamental field. In this sense, the probe scheme makes no assumptions about the motion along the fundamental field. In practice, applying the Coulomb-corrected scheme is not significantly more difficult than the original scheme. Experimentally, it is challenging to measure the absolute value of the two-color delay as one typically measures only the variation of the optimal phases with harmonic order. In this case, additional assumptions are needed to obtain the ionization time, see [26]. The same can be done in combination with the scheme presented here. Hence, we conclude that the proposed scheme is well suited to reveal the Coulomb shift of the ionization time in an experiment.

ACKNOWLEDGMENTS

This work has been supported by the National Natural Science Foundation of China (Grants No. 12204209, No. 12274188, and No. 12064023).

APPENDIX: ADIABATIC MODEL

In this appendix, we describe the adiabatic model for the Coulomb effect on the ionization and return times of HHG. Here, only the linearly polarized fundamental field $E_x(t)$ is considered,

$$E_x(t) = -\frac{\partial A_x(t)}{\partial t} = E_0 \cos(\omega t) \tag{A1}$$

with the vector potential $A_x(t) = -E_0 \sin(\omega t)/\omega$. In the model, the electron travels along a classical trajectory between the real times τ_i (ionization time) and τ_r (return time). The term "adiabatic" refers to the initial conditions of the trajectories: (i) the initial position is chosen as the tunnel exit in the static-field limit of tunneling through a triangular barrier; (ii) the Coulomb potential is taken into account by choosing a nonzero initial velocity equal to the Coulomb-induced momentum change acquired by an outgoing electron under the assumption of a static electric field. In detail, the electron trajectory

starts at the tunnel exit $x_i = -I_p/E_x(\tau_i)$ and it ends at the position $x_r = 0$, since recollision with the parent ion is required for HHG. Except for the above-mentioned choice of initial velocity, the Coulomb force is neglected so that the displacement between τ_i and τ_r can be expressed as

$$x_r - x_i = \int_{\tau_i}^{\tau_r} \left[p_x(\tau_i, \tau_r) + A_x(t)\right] dt \tag{A2}$$

with the canonical momentum

$$p_x(\tau_i, \tau_r) = \frac{x_r - x_i}{\tau_r - \tau_i} - \frac{1}{\tau_r - \tau_i} \int_{\tau_i}^{\tau_r} A_x(t)\, dt. \tag{A3}$$

In terms of the canonical momentum, the initial velocity at τ_i is

$$v_x(\tau_i) = p_x(\tau_i, \tau_r) + A_x(\tau_i) \tag{A4}$$

and the final velocity at τ_r is

$$v_x(\tau_r) = p_x(\tau_i, \tau_r) + A_x(\tau_r). \tag{A5}$$

The initial velocity is set equal to the adiabatic Coulomb-induced velocity change along the x axis [44, 50]

$$v_x\left(\tau_i\right) = \alpha \frac{\pi E_x(\tau_i)}{\left(2I_p\right)^{3/2}}. \tag{A6}$$

where α denotes the Coulomb interaction strength: $\alpha = 1$ is the case of the full Coulomb interaction; $\alpha = 0$ represents the Coulomb-free case. For $\alpha = 0$, we denote the ionization and return times as τ_i^0 and τ_r^0. In order to generate the harmonic frequency Ω, the electron must return with the velocity

$$v_x(\tau_r) = v_r = \sqrt{2\left(\Omega - I_p\right)}, \tag{A7}$$

where we choose a positive sign, assuming that the electron returns from the negative side. This implies that the field at the ionization time is positive, $E_x(\tau_i) > 0$.

From Eqs. (A4),(A5),(A6),(A7), we derive that, to first order in the Coulomb interaction, the ionization and return times must change (relative to the Coulomb-free case) by $d\tau_i$ and $d\tau_r$ that satisfy

$$dv_x\left(\tau_i\right) = \alpha \frac{\pi E_x(\tau_i^0)}{\left(2I_p\right)^{3/2}} = \left.\frac{\partial p_x}{\partial \tau_i}\right|_{\tau_i^0,\tau_r^0} d\tau_i + \left.\frac{\partial p_x}{\partial \tau_r}\right|_{\tau_i^0,\tau_r^0} d\tau_r + \left.\frac{\partial A_x(\tau_i)}{\partial \tau_i}\right|_{\tau_i^0} d\tau_i, \tag{A8}$$

and

$$dv_x\left(\tau_r\right) = 0 = \left.\frac{\partial p_x}{\partial \tau_i}\right|_{\tau_i^0,\tau_r^0} d\tau_i + \left.\frac{\partial p_x}{\partial \tau_r}\right|_{\tau_i^0,\tau_r^0} d\tau_r + \left.\frac{\partial A_x(\tau_r)}{\partial \tau_r}\right|_{\tau_r^0} d\tau_r. \tag{A9}$$

Solving Eqs. (A8) and (A9), we obtain the Coulomb-induced ionization time shift

$$d\tau_i = -\frac{\alpha\pi}{\left(2I_p\right)^{3/2}} \times \frac{\left(\tau_r^0 - \tau_i^0\right) E_x(\tau_r^0) + v_r}{\left(\tau_r^0 - \tau_i^0\right) E_x(\tau_r^0) + v_r + \frac{I_p \dot{E}_x\left(\tau_i^0\right) E_x(\tau_r^0)}{E_x^3\left(\tau_i^0\right)}} \tag{A10}$$

and the return time shift

$$d\tau_r = \frac{\alpha\pi}{\left(2I_p\right)^{3/2}} \times \frac{I_p \dot{E}_x(\tau_i^0)/E_x^2(\tau_i^0)}{(\tau_r^0 - \tau_i^0) E_x(\tau_r^0) + v_r + \frac{I_p \dot{E}_x(\tau_i^0) E_x(\tau_r^0)}{E_x^3\left(\tau_i^0\right)}}. \tag{A11}$$

The terms involving the time derivative of the field originate from

$$\left.\frac{\partial x_i}{\partial \tau_i}\right|_{\tau_i^0} = I_p\, \dot{E}_x(\tau_i^0)/E_x^2(\tau_i^0). \tag{A12}$$

If the tunnel exit is instead chosen independent of the ionization time, i.e., $\left.\frac{\partial x_i}{\partial \tau_i}\right|_{\tau_i^0} = 0$, we arrive at the simple adiabatic correction $d\tau_i = -\alpha\pi/\left(2I_p\right)^{3/2}$ used in [35] and vanishing return time shift $d\tau_r = 0$. Compared to the simple adiabatic correction, the ionization time obtained from Eq. (A10) is shifted to slightly earlier values with the difference varying between ~ 2 attoseconds and ~ 7 attoseconds.

Finally, the actual ionization and return times of the adiabatic model are obtained by adding the shifts $d\tau_i$ and $d\tau_r$ to the values obtained from the Coulomb-free QO model.

[1] P. B. Corkum and F. Krausz, Attosecond science, Nat. Phys. **3**, 381 (2007).

[2] S. Pabst and R. Santra, Spin–orbit effects in atomic high-harmonic generation, J. Phys. B: At. Mol. Opt. Phys. **47**, 124026 (2014).

[3] P. M. Kraus, B. Mignolet, D. Baykusheva, A. Rupenyan, L. Horný, E. F. Penka, G. Grassi, O. I. Tolstikhin, J. Schneider, F. Jensen, L. B. Madsen, A. D. Bandrauk, F. Remacle, and H. J. Wörner, Measurement and laser control of attosecond charge migration in ionized iodoacetylene, Science **350**, 790 (2015).

[4] P. Lan, M. Ruhmann, L. He, C. Zhai, F. Wang, X. Zhu,

Q. Zhang, Y. Zhou, M. Li, M. Lein, and P. Lu, Attosecond probing of nuclear dynamics with trajectory-resolved high-harmonic spectroscopy, Phys. Rev. Lett. **119**, 033201 (2017).
[5] L. He, Q. Zhang, P. Lan, W. Cao, X. Zhu, C. Zhai, F. Wang, W. Shi, M. Li, X.-B. Bian, P. Lu, and A. D. Bandrauk, Monitoring ultrafast vibrational dynamics of isotopic molecules with frequency modulation of high-order harmonics, Nat. Commun. **9**, 1108 (2018).
[6] S. Yue, S. Brennecke, H. Du, and M. Lein, Probing dynamical symmetries by bicircular high-order harmonic spectroscopy beyond the Born-Oppenheimer approximation, Phys. Rev. A **101**, 053438 (2020).
[7] H. Lakhotia, H. Y. Kim, M. Zhan, S. Hu, S. Meng, and E. Goulielmakis, Laser picoscopy of valence electrons in solids, Nature **583**, 55 (2020).
[8] N. Mayer, S. Beaulieu, A. Jiménez-Galán, S. Patchkovskii, O. Kornilov, D. Descamps, S. Petit, O. Smirnova, Y. Mairesse, and M. Y. Ivanov, Role of spin-orbit coupling in high-order harmonic generation revealed by supercycle Rydberg trajectories, Phys. Rev. Lett. **129**, 173202 (2022).
[9] P. B. Corkum, Plasma perspective on strong field multiphoton ionization, Phys. Rev. Lett. **71**, 1994 (1993).
[10] K. C. Kulander, K. J. Schafer, and J. L. Krause, Dynamics of short-pulse excitation, ionization and harmonic conversion, in *Super-Intense Laser-Atom Physics,* edited by B. Pireaux, A. L'Huillier and K. Rzążewski, NATO ASI, Series B: Physics (Springer, Boston, 1993), Vol. 316.
[11] M. Lewenstein, P. Balcou, M. Y. Ivanov, A. L'Huillier, and P. B. Corkum, Theory of high-harmonic generation by low-frequency laser fields, Phys. Rev. A **49**, 2117 (1994).
[12] B. C. P. Salières, L. L. Déroff, F. Grasbon, G. G. Paulus, H. Walther, R. Kopold, W. Becker, D. B. Milošević, A. Sanpera, and M. Lewenstein, Feynman's path-integral approach for intense-laser-atom interactions, Science **292**, 902 (2001).
[13] O. Raz, O. Pedatzur, and N. Dudovich, Spectral caustics in attosecond science, Nat. Photon. **6**, 170 (2012).
[14] D. Faccialà, S. Pabst, B. D. Bruner, A. G. Ciriolo, S. De Silvestri, M. Devetta, M. Negro, H. Soifer, S. Stagira, N. Dudovich, and C. Vozzi, Probe of multielectron dynamics in xenon by caustics in high-order harmonic generation, Phys. Rev. Lett. **117**, 093902 (2016).
[15] V. A. Birulia and V. V. Strelkov, Spectral caustic in two-color high-order harmonic generation: Role of Coulomb effects, Phys. Rev. A **99**, 043413 (2019).
[16] M. Lein, Attosecond probing of vibrational dynamics with high-harmonic generation, Phys. Rev. Lett. **94**, 053004 (2005).
[17] S. Baker, J. S. Robinson, C. Haworth, H. Teng, R. Smith, C. C. Chirilă, M. Lein, J. Tisch, and J. P. Marangos, Probing proton dynamics in molecules on an attosecond time scale, Science **312**, 424 (2006).
[18] D. Baykusheva, M. S. Ahsan, N. Lin, and H. J. Wörner, Bicircular high-harmonic spectroscopy reveals dynamical symmetries of atoms and molecules, Phys. Rev. Lett. **116**, 123001 (2016).
[19] O. Pedatzur, G. Orenstein, V. Serbinenko, H. Soifer, B. D. Bruner, A. J. Uzan, D. S. Brambila, A. G. Harvey, L. Torlina, F. Morales, O. Smirnova, and N. Dudovich, Attosecond tunnelling interferometry, Nat. Phys. **11**, 815 (2015).
[20] O. Kneller, D. Azoury, Y. Federman, M. Krüger, A. J. Uzan, G. Orenstein, B. D. Bruner, O. Smirnova, S. Patchkovskii, M. Ivanov, and N. Dudovich, A look under the tunnelling barrier via attosecond-gated interferometry, Nat. Phys. **16**, 304 (2022).
[21] M. Kitzler and M. Lezius, Spatial control of recollision wave packets with attosecond precision, Phys. Rev. Lett. **95**, 253001 (2005).
[22] M. Richter, M. Kunitski, M. Schöffler, T. Jahnke, L. P. H. Schmidt, M. Li, Y. Q. Liu, and R. Dörner, Streaking temporal double-slit interference by an orthogonal two-color laser field, Phys. Rev. Lett. **114**, 143001 (2015).
[23] N. Eicke and M. Lein, Analysis of electron trajectories with two-color strong-field ionization, J. Mod. Opt. **64**, 981 (2017).
[24] M.-M. Liu, M. Han, P. Ge, C. He, Q. Gong, and Y. Liu, Strong-field ionization of diatomic molecules in orthogonally polarized two-color fields, Phys. Rev. A **97**, 063416 (2018).
[25] D. B. Milošević and W. Becker, X-ray harmonic generation by orthogonally polarized two-color fields: Spectral shape and polarization, Phys. Rev. A **100**, 031401(R) (2019).
[26] D. Shafir, H. Soifer, B. D. Bruner, M. Dagan, Y. Mairesse, S. Patchkovskii, M. Y. Ivanov, O. Smirnova, and N. Dudovich, Resolving the time when an electron exits a tunnelling barrier, Nature (London) **485**, 343 (2012).
[27] J. Zhao and M. Lein, Determination of ionization and tunneling times in high-order harmonic generation, Phys. Rev. Lett. **111**, 043901 (2013).
[28] T. Brabec, M. Y. Ivanov, and P. B. Corkum, Coulomb focusing in intense field atomic processes, Phys. Rev. A **54**, R2551 (1996).
[29] A. Gordon, R. Santra, and F. X. Kärtner, Role of the Coulomb singularity in high-order harmonic generation, Phys. Rev. A **72**, 063411 (2005).
[30] S. V. Popruzhenko and D. Bauer, Strong field approximation for systems with Coulomb interaction, J. Mod. Opt. **55**, 2573 (2008).
[31] T.-M. Yan, S. V. Popruzhenko, M. J. J. Vrakking, and D. Bauer, Low-energy structures in strong field ionization revealed by quantum orbits, Phys. Rev. Lett. **105**, 253002 (2010).
[32] A. S. Landsman, C. Hofmann, A. N. Pfeiffer, C. Cirelli, and U. Keller, Unified approach to probing Coulomb effects in tunnel ionization for any ellipticity of laser light, Phys. Rev. Lett. **111**, 263001 (2013).
[33] L. Torlina and O. Smirnova, Coulomb time delays in high harmonic generation, New J. Phys. **19**, 023012 (2017).
[34] M. V. Frolov, N. L. Manakov, A. A. Minina, S. V. Popruzhenko, and A. F. Starace, Adiabatic-limit Coulomb factors for photoelectron and high-order-harmonic spectra, Phys. Rev. A **96**, 023406 (2017).
[35] S. Yue, S. Xue, H. Du, and M. Lein, Revealing Coulomb time shifts in high-order harmonic generation by frequency-dependent streaking, Phys. Rev. A **105**, L041103 (2022).
[36] S. Yue, Y. Li, S. Xue, H. Du, and M. Lein, Ionization and recombination times of the long trajectory in high-order harmonic generation, Phys. Rev. A **106**, 023117 (2022).
[37] J. Crank and P. Nicolson, A practical method for numerical evaluation of solutions of partial differential equations of the heat-conduction type, Proc. Cambridge Phi-

los. Soc. **43**, 50 (1947).
[38] M. Nurhuda and F. H. M. Faisal, Numerical solution of time-dependent schrödinger equation for multiphoton processes: A matrix iterative method, Phys. Rev. A **60**, 3125 (1999).
[39] P. Ehrenfest, Bemerkung über die angenäherte Gültigkeit der klassischen Mechanik innerhalb der Quantenmechanik, Zeitschrift für Physik **45**, 455 (1927).
[40] N. Dudovich, O. Smirnova, J. Levesque, Y. Mairesse, M. Y. Ivanov, D. Villeneuve, and P. B. Corkum, Measuring and controlling the birth of attosecond XUV pulses, Nat. Phys. **2**, 781 (2006).
[41] X. Zhou, R. Lock, W. Li, N. Wagner, M. M. Murnane, and H. C. Kapteyn, Molecular recollision interferometry in high harmonic generation, Phys. Rev. Lett. **100**, 073902 (2008).
[42] C. C. Chirilă, I. Dreissigacker, E. V. van der Zwan, and M. Lein, Emission times in high-order harmonic generation, Phys. Rev. A **81**, 033412 (2010).
[43] B. Zhang and M. Lein, High-order harmonic generation from diatomic molecules in an orthogonally polarized two-color laser field, Phys. Rev. A **100**, 043401 (2019).
[44] N. I. Shvetsov-Shilovski, S. P. Goreslavski, S. V. Popruzhenko, and W. Becker, Capture into Rydberg states and momentum distributions of ionized electrons, Laser Phys. **19**, 1550 (2009).
[45] M. Y. Ivanov, M. Spanner, and O. Smirnova, Anatomy of strong field ionization, J. Mod. Opt. **52**, 165 (2005).
[46] F. Krausz and M. Ivanov, Attosecond physics, Rev. Mod. Phys. **81**, 163 (2009).
[47] D. Shafir, Y. Mairesse, D. M. Villeneuve, P. B. Corkum, and N. Dudovich, Atomic wavefunctions probed through strong-field light–matter interaction, Nat. Phys. **5**, 412 (2009).
[48] E. V. van der Zwan and M. Lein, Molecular imaging using high-order harmonic generation and above-threshold ionization, Phys. Rev. Lett. **108**, 043004 (2012).
[49] L. V. Keldysh, Ionization in the field of a strong electromagnetic wave, Sov. Phys. JETP **20**, 1307 (1965).
[50] S. P. Goreslavski, G. G. Paulus, S. V. Popruzhenko, and N. I. Shvetsov-Shilovski, Coulomb asymmetry in above-threshold ionization, Phys. Rev. Lett. **93**, 233002 (2004).